Research Article | Vol. 26, No. 15 | 23 Jul 2018 | OPTICS EXPRESS 18863
Optics EXPRESS

Calibration of an in-water multi-excitation fluorometer for the measurement of phytoplankton chlorophyll-a fluorescence quantum yield

Derek J. Griffith,[1,*] Emma L. Bone,[2,3,4,5] Sandy J. Thomalla,[2,4] and Stewart Bernard[2,5]

[1] *Optronic Sensor Systems (OSS), Defence, Peace, Safety and Security (DPSS), Council for Scientific and Industrial Research, P. O. Box 395, Pretoria 0001, South Africa*
[2] *Marine Research Institute, Department of Oceanography, University of Cape Town, Rondebosch 7700, South Africa*
[3] *Nansen-Tutu Centre for Marine Environmental Research, Marine Research Institute, University of Cape Town, South Africa*
[4] *Southern Ocean Carbon and Climate Observatory, Natural Resources and the Environment, Council for Scientific and Industrial Research, Rosebank 7700, South Africa*
[5] *Earth Observation, Natural Resources and the Environment, Council for Scientific and Industrial Research, Rosebank 7700, South Africa*
[*] *dgriffith@csir.co.za*
http://www.csir.co.za

Abstract: A multi-excitation fluorometer (MFL, JFE Advantech Co., Ltd.), originally designed to discriminate between phytoplankton species present within a population, has been redirected for use in fluorescence quantum yield (FQY) determination. While this calibration for apparent FQY requires no modification of the MFL, it is necessary to have an independent measurement of the spectral absorption coefficient of the subject fluid. Two different approaches to calibration were implemented. The primary method made use of reference fluorescent dye solutions of known quantum yield. The second method made use of acrylic fluorescent plaques and films. The two methods yielded consistent results, except in the 570 and 590 nm LED channels of the MFL. Application of the MFL in FQY determination is illustrated with an *in situ* Southern Ocean sample.

© 2018 Optical Society of America under the terms of the OSA Open Access Publishing Agreement

OCIS codes: (010.0280) Remote sensing and sensors; (010.4450) Oceanic optics; (300.6280) Spectroscopy, fluorescence and luminescence.

References and links

1. A. Morel and A. Bricaud, "Theoretical results concerning light absorption in a discrete medium, and application to specific absorption of phytoplankton," Deep. Sea Res. Part A **28**, 1375–1393 (1981).
2. L. N. M. Duysens, "The flattening of the absorption spectrum of suspensions, as compared to that of solutions," Biochim.Biophys. Acta **19**, 1–12 (1956).
3. A. Bricaud, M. Babin, A. Morel, and H. Claustre, "Variability in the chlorophyll-specific absorption coefficients of natural phytoplankton," J. Geophys. Res. **100**, 13321–13332 (1995).
4. S. Sathyendranath, L. Lazzara, and L. Prieur, "Variations in the spectral values of specific absorption of phytoplankton," Limnol. Oceanogr. **32**, 403–415 (1987).
5. V. Stuart, S. Sathyendranath, T. Platt, H. Maass, and B. D. Irwin, "Pigments and species composition of natural phytoplankton populations: effect on the absorption spectra," J. Plankton Res. **20**, 187–217 (1998).
6. S. E. Lohrenz, A. Weidemann, and M. Tuel, "Phytoplankton spectral absorption as influenced by community size structure and pigment composition," J. Plankton Res. **25**, 35–61 (2003).
7. P. G. Falkowski and J. A. Raven, *Aquatic Photosynthesis* (Princeton University, 2007), chap. 2.
8. W. J. Vredenberg and L. Slooten, "Chlorophyll a fluorescence and photochemical activities of chloroplast fragments," Biochim. Biophys. Acta **143**, 583–594 (1967).
9. G. H. Krause and E. Weis, "Chlorophyll fluorescence and photosynthesis: The basics," Annu. Rev. Plant Physiol. Plant Mol. Biol. **42**, 313–349 (1991).

#323319 https://doi.org/10.1364/OE.26.018863
Journal © 2018 Received 14 Mar 2018; revised 26 Apr 2018; accepted 27 Apr 2018; published 10 Jul 2018

Optics EXPRESS

10. V. Lutz and S. Sathyendaranath, "Changes in the in vivo absorption and fluorescence excitation spectra with growth irradiance in three species of phytoplankton," J. Plankton Res. **23**, 555–569 (2001).
11. S. Maritorena, A. Morel, and B. Gentili, "Determination of the fluorescence quantum yield by oceanic phytoplankton in their natural habitat." Appl. Opt. **39**, 6725–37 (2000).
12. J. R. Morrison, "In situ determination of the quantum yield of phytoplankton chlorophyll a fluorescence: A simple algorithm, observations, and a model," Limnol. Oceanogr. **48**, 618–631 (2003).
13. M. Babin, A. Morel, and B. Gentili, "Remote sensing of sea surface sun-induced chlorophyll fluorescence: consequences of natural variations in the optical characteristics of phytoplankton and the quantum yield of chlorophyll a fluorescence," Int. J. Remote. Sens. **17**, 2417–2448 (1996).
14. M. J. Behrenfeld, T. K. Westberry, E. S. Boss, R. T. O'Malley, D. A. Siegel, J. D. Wiggert, B. A. Franz, C. R. McClain, G. C. Feldman, S. C. Doney, J. K. Moore, G. Dall'Olmo, A. J. Milligan, I. Lima, and N. Mahowald, "Satellite-detected fluorescence reveals global physiology of ocean phytoplankton," Biogeosciences. **6**, 779–794 (2009).
15. R. A. Desiderio, C. M. Moore, C. Lantz, and T. J. Cowles, "Multiple excitation fluorometer for in situ oceanographic applications," Appl. Opt. **36**, 1289–1296 (1997).
16. M. Beutler, K. H. Wiltshire, B. Meyer, C. Moldaenke, C. Lüring, M. Meyerhöfer, U.-P. Hansen, and H. Dau, "A fluorometric method for the differentiation of algal populations in vivo and in situ," Photosynth. Res. **72**, 39–53 (2002).
17. M. Beutler, K. H. Wiltshire, M. Arp, J. Kruse, C. Reineke, C. Moldaenke, and U. P. Hansen, "A reduced model of the fluorescence from the cyanobacterial photosynthetic apparatus designed for the in situ detection of cyanobacteria," Biochim. Biophys. Acta **1604**, 33 – 46 (2003).
18. M. Yoshida, T. Horiuchi, and Y. Nagasawa, "In situ multi-excitation chlorophyll fluorometer for phytoplankton measurements: Technologies and applications beyond conventional fluorometers," in *Proceedings of the OCEANS* (IEEE, 2011), pp. 1–4.
19. M. Ostrowska, "Dependence between the quantum yield of chlorophyll a fluorescence in marine phytoplankton and trophicity in low irradiance level," Opt. Appl. **41**, 567–577 (2011).
20. J. N. Demas and G. A. Crosby, "Measurement of Photoluminescence Quantum Yields. A Review," The J. Phys. Chem. **75**, 991–1024 (1971).
21. C. S. Yentsch, "Measurement of visible light absorption by particulate matter in the ocean," Limnol. Oceanogr. **7**, 207–217 (1962).
22. M. Kishino, M. Takahashi, N. Okami, and S. Ichimura, "Estimation of the Spectral Absorption Coefficients of Phytoplankton in the Sea," Bull. Mar. Sci. **37**, 634–642 (1985).
23. C. S. Roesler, "Theoretical and experimental approaches to improve the accuracy of particulate absorption coefficients derived from the quantitative filter technique," Limnol. Oceanogr. **43**, 1649–1660 (1998).

1. Introduction and background

The light reactions of photosynthesis take place in two characteristic pigment-protein/ electron-carrier systems, known as photosystem (PS) I and II. These photosystems are equipped with a network of light-harvesting antennae pigments, which function solely to extend the range of light absorption. The absorption spectrum of a specific phytoplankton species is representative of the total absorption by all pigment-protein complexes within the cell. This includes photoprotective pigments, present within phytoplankton to aid in the dissipation of excess photon energy under high light conditions.

Cell size and pigment composition and concentration, are known to affect the absorption efficiency of phytoplankton [1]. An increase in cell volume or intracellular pigment concentration leads to a reduction in the phytoplankton absorption efficiency due to the arrangement of pigments within chloroplasts, and chloroplasts within the cells. This phenomenon is known as the "package effect" [2], and is responsible for lowering the absorption coefficient of phytoplankton per unit of chlorophyll-*a* (chl-*a*) [3]. Pigment composition and packaging are the main drivers of variation in phytoplankton-specific coefficients [4–6].

Chlorophyll-*a* absorbs light in the blue and red parts of the visible electromagnetic spectrum (400 -700 nm), which elevates the molecule to an excited vibrational state. The return of excited chl-*a* to the ground state occurs either through photochemistry, non-radiative decay or re-emission as light, i.e. fluorescence [7]. At room temperature, chl-*a* fluorescence is predominantly emitted by PSII and associated light harvesting complexes [8], and is observed as a typically conserved distribution around 685 nm [9]. Phytoplankton fluorescence excitation spectra are derived exclusively from the re-emission of light reaching chl-*a* of PSII. The fixed waveband

Optics EXPRESS

of fluorescence varies with incident light as a function of wavelength, largely determined by specifics composition, physiological state and level of photoadaptation [10].

The natural fluorescence of chl-*a* is important to the non-invasive study of phytoplankton dynamics in their native environment. The quantum yield of chl-*a* fluorescence (Φ_F), i.e. the ratio of photons emitted as fluorescence to those absorbed by the cell, provides a first order measure of photosynthetic efficiency. The derivation of Φ_F requires, aside from precise quantification of the fluorescence signal, that the spectral characteristics of the excitation energy and the spectral absorption capacity of the phytoplankton be known. The Φ_F in natural phytoplankton assemblages is considered an apparent Φ_F, largely due to the contribution of PSI antennae pigments and photoprotective carotenoids towards phytoplankton-specific absorption and not PSII fluorescence. Chlorphyll-*a* fluorescence quantum yield may be derived from *in situ* measurements [11, 12] or remotely through satellite ocean colour sensors [13, 14].

Multi-excitation fluorometers, typically used to discriminate between phytoplankton taxa within a community [15–18], have been identified as a possible option for use in apparent Φ_F determination [19]. The present study describes the characterization and absolute radiometric calibration of a JFE Advantech Co., Ltd. Multi-Exciter Fluorometer (MFL, model MFL10W-CAD, SN. 0013). The MFL consists of nine excitation light-emitting diodes (LEDs, 375, 400, 420, 435, 470, 505, 525, 570 and 590 nm) and detects emitted light between 640-1000 nm. Characterized excitation LEDs and the resultant fluorescence emission, together with *in situ* phytoplankton-specific absorption data, allow for the derivation of the Φ_F. The nine excitation wavelengths allows for unique taxonomic resolution, providing insight into the influence of phytoplankton community structure on Φ_F. An improved understanding of the drivers of Φ_F variability will shape the development of novel sensors and advance existing ocean colour algorithms.

2. Calibration methods

The MFL was characterized in as much detail as possible, including measurement of LED spectra (Fig. 1), spatial distribution of illumination, LED temporal cycles, detector field of view (FOV) and zero bias over temperature. The instrument was then calibrated for quantum yield using two distinct methodologies, where the primary and most direct method made use of fluorescent dye solutions of known quantum yield and spectral characteristics. The second method utilized fluorescent acrylic plaques and films to determine the response of the MFL as a function of distance. The MFL was originally calibrated by the manufacturer against a solution of Rhodamine WT dye, with the raw output signal R expressed as the equivalent signal from Rhodamine WT dye of specific dilution in parts-per-billion (ppb in water). Since we were unable to obtain sufficient quantitative information on the fluorescence of Rhodamine WT, we did not attempt to exploit this calibration. The MFL is assumed to have a linear radiometric response that is also stable with temperature. All calibrations described here were executed at an ambient temperature of 20 ± 2 °C. All radiometric quantities are photon-based. The symbols and associated units of measurement for this work are provided in Table 1.

2.1. Fluorescent dye method

Water-soluble fluorescent dyes of known quantum yield and high photostability were sought, with an emission spectrum similar to that of chlorophyll and excitation spectrum covering the full stimulation range of the MFL (350 to 610 nm). Large Stokes shift (minimal overlap of the excitation and emission spectra of the dye) was considered advantageous in order to reduce second and higher order excitation light field effects. Ideal characteristics for quantum yield standard dyes are reviewed by Demas and Crosby [20].

The carboxy derivatives of two suitable ATTO-TEC dyes with different spectral characteristics were selected, namely ATTO655 and ATTO490LS, the latter having an exceptionally large Stokes shift. These dyes both have a specified quantum yield of 0.3, but full uncertainty data was not

Optics EXPRESS

available from ATTO-TEC. The absorption spectra of these dyes, together with measured LED photon spectra are shown in Fig. 1.

Table 1. Symbols and Units

Symbol	Quantity	Typical Units
$A(\lambda)$	Spectral absorbance (spectral optical density)	
a_{ij}	Absorption coefficient of solution i over LED j spectrum	cm^{-1}
$a_i(\lambda)$	Spectral absorption coefficient of calibration solution i	cm^{-1}
$a_j^\star$	Phytoplankston-specific absorption coefficient, LED j	cm^{-1}
c_i	Molar concentration of calibration solution i	mol L^{-1}
E_λ	Spectral photon irradiance	s^{-1} cm^{-2} nm^{-1}
$g_j(z)$	Distance calibration functions for MFL, LED j	MFLu
k_{ij}	MFL calibration constant for solution i, LED j	MFLu cm
ℓ	Physical path length in spectrophotometer cuvettes	cm
L	Photon radiance	s^{-1} sr^{-1} cm^{-2}
n	Refractive index	
p_i	MFL-relative partial quantum yield factor for solution i	
p_c	MFL-relative partial quantum yield factor for chlorophyll	
$\mathfrak{R}(\lambda)$	MFL sensor relative quantum spectral response	
R_{ij}	MFL output response to solution i, in LED channel j	MFLu
R_j	MFL field measurement data, LED channel j	MFLu
$\mathcal{S}_i(\lambda)$	Relative fluorescent emission spectrum for solution i	
t	Physical thickness	cm
$\mathcal{T}(\lambda)$	Spectral transmittance	
$\mathcal{T}_{fj}$	Effective filter transmittance for LED channel j	
V	Volume	mL or cm^3
$\varepsilon_i(\lambda)$	Spectral molar absorptivity of solution i	M^{-1} cm^{-1}
ε_{ij}	Molar absorptivity of solution i in LED channel j	M^{-1} cm^{-1}
$\varsigma_j(\lambda)$	Relative LED emission spectrum for LED channel j	
λ	Wavelength	nm
Φ_i	Total fluorescence quantum yield for solution i	
Φ_λ	Spectral photon flux	s^{-1} nm^{-1}
Φ	Total photon flux	s^{-1}

2.1.1. Linear calibration model

The linear calibration model for the MFL output signal response to a fluorescent solution with index i was written as

$$R_{ij} = k_{ij} a_{ij} p_i \Phi_i, \tag{1}$$

where

- R_{ij} is the MFL signal response (in "equivalent ppb Rhodamine", but we assumed the response unitless, written "MFLu"), to the fluorescent solution i exposed to LED wavelength (spectral distribution) j,
- a_{ij} is the absorption coefficient of solution i, a mean value weighted by the spectral photon distribution of LED j,

Optics EXPRESS

- k_{ij} is a calibration constant for solution i, LED j, expected to be independent of solution i, leaving k_j,
- p_i is the MFL-relative partial quantum yield factor for the fluorophore in solution i (described in Section 2.1.3) and
- Φ_i is the total FQY for the fluorophore in solution i.

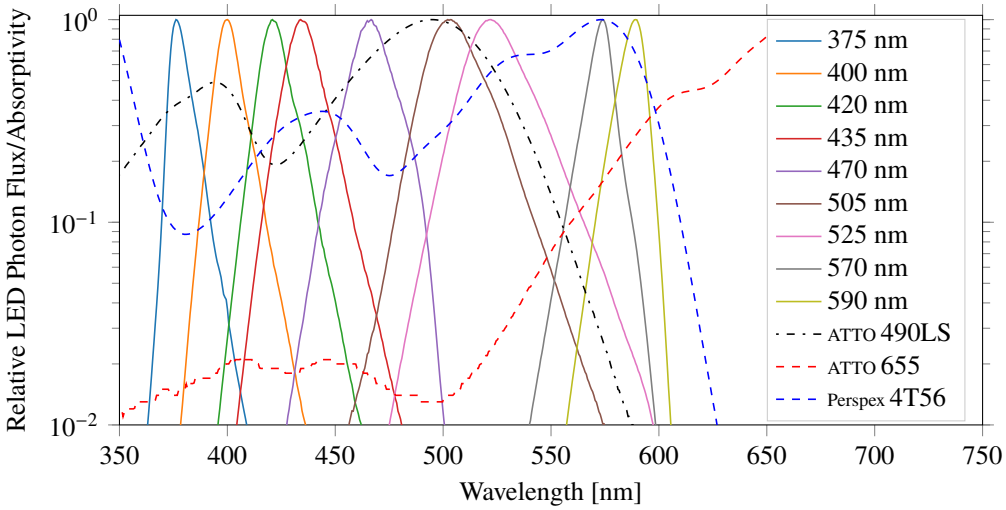

Fig. 1. MFL LED normalized photon spectra, plotted on a log scale with ATTO-TEC Dye and Perspex 4T56 relative spectral absorptivity.

The linear calibration process establishes the calibration constants k_{ij} determined as

$$k_{ij} = \frac{R_{ij}}{a_{ij} p_i \Phi_i}. \tag{2}$$

A stepwise description of the linear calibration is as follows: (1) The spectral molar absorptivity $\varepsilon_i(\lambda)$ of the working dye stock solutions was determined using a Varian (now Agilent) Cary 500 spectrophotometer and compared to the data supplied by the manufacturer. (2) The MFL was immersed in solutions of the working stock at known dilution ratios under the assumption that the absorption coefficients were linearly related to concentration. The R_{ij} values were established by immersing the MFL in a fluorescent solution index i (the dyes ATTO655 or ATTO490LS dissolved in deionized water (dH_2O)), where the equivalent absorption coefficient a_{ij} for each LED spectral photon distribution had been established. A time-averaged response R_{ij} of the MFL was measured for each solution. (3) The LED-specific absorption coefficients of the calibration dye solutions were calculated using spectral weighted averaging. To get good signal on all channels of the MFL, solutions of the dyes at various concentrations were used. A stock dye solution of known spectral absorption coefficient was made up using dH_2O, from which we could calculate a_{ij} for any diluted solution of the stock (see Section 2.1.2). (4) The MFL partial quantum yield was determined (see Section 2.1.3). This was necessary as part of the dye emission spectrum is filtered out by the MFL cut-on filter. (5) Finally, the calibration coefficient for each LED wavelength was computed using Eq. (2).

Optics EXPRESS

2.1.2. Dye characterization

A Cary 500 spectrophotometer, with long path ($\ell = 10\,\mathrm{cm}$) cuvettes, was used to determine the spectral molar absorptivity of the dye, and hence the spectral molar absorption coefficient of any dye solutions used for calibration purposes. The FQY Φ_i of the dyes was supplied by the manufacturer. The spectral molar absorptivity, $\varepsilon(\lambda)$ is an inherent characteristic of the dye and does not depend on concentration. The transmission $\mathcal{T}$ of the solution in the cuvette was measured to determine the absorbance A (also known as optical density), related as

$$A(\lambda) = -\log_{10}\mathcal{T}(\lambda) = \varepsilon(\lambda)\ell c, \tag{3}$$

where c is the molar concentration of the dye solution. The absorbance of the working stock, $A_0(\lambda)$ was determined spectrophotometrically by measuring the transmission of the working stock at various dilution ratios. This became necessary as the working stock absorbance was too high in some spectral regions to be measured reliably at full concentration c_0. From Eq. (3) it follows that

$$A(\lambda) = A_0(\lambda)\frac{c}{c_0}. \tag{4}$$

Eq. (4) was exploited by fitting a straight line to the measured absorbance of solutions at known working stock dilution ratios. The working stock absorbance was determined by extrapolating the fitted line to $c/c_0 = 1$.

The effective molar absorptivity for the dye in solution i for LED spectral channel j was computed by taking an integral, weighted by the LED photon spectrum $\varsigma_j(\lambda)$ as

$$\varepsilon_{ij} = \frac{\int \varepsilon_i(\lambda)\varsigma_j(\lambda)\mathrm{d}\lambda}{\int \varsigma_j(\lambda)\mathrm{d}\lambda}. \tag{5}$$

The LED spectra $\varsigma_j(\lambda)$ were measured using an Avantes spectrometer with calibrated fiber-optic spectral irradiance attachment. The absorption coefficient for solution i which has molar concentration c_i and for LED spectrum j, was calculated as

$$a_{ij} = \varepsilon_{ij}c_i \ln 10. \tag{6}$$

2.1.3. MFL-relative partial quantum yield

The MFL-relative partial quantum yield factor lies in the range 0 to 1 and takes into account the spectral response of the MFL detector channel. Suppose the relative spectral quantum response of the MFL is denoted $\mathfrak{R}(\lambda)$ and the emission spectrum of fluorescent solution i is denoted $\mathcal{S}_i(\lambda)$, then the MFL-relative partial quantum yield factor is defined as

$$p_i \equiv \frac{\int \mathcal{S}_i(\lambda)\mathfrak{R}(\lambda)\mathrm{d}\lambda}{\int \mathcal{S}_i(\lambda)\mathrm{d}\lambda}. \tag{7}$$

The quantum response $\mathfrak{R}(\lambda)$ of the MFL was provided by the manufacturer and the dye emission spectra $\mathcal{S}_i(\lambda)$ are published by ATTO-TEC. Both are shown in Fig. 2 . The MFL-relative partial quantum yield factors calculated in this way and used in this calibration are provided in Table 2. For chlorophyll, the MFL-relative partial quantum yield factor was taken as the mean of the values for solution in ether and MeOH, that is, $p_c = 0.851$.

2.2. Linear calibration application

In field usage, Eq. (2) is solved for Φ and a set of field-station, time-averaged MFL measurements R_j are input (data were continuously recorded for 10 sec every 1 min, over a 20 min period). The calibration factors k_j have been provided by the dye calibration, and the LED channel

Optics EXPRESS

Table 2. MFL-Relative Partial Quantum Yield Factors

Fluorophore	p_i Photon-Based
ATTO 490LS	0.624
ATTO 655	0.893
Chl-a in Ether	0.827
Chl-a in MeOH	0.875
Perspex 4T56	0.319

phytoplankton-specific absorption coefficients $a_j^\star$ have come from independent field measurements of the sample spectral absorption, determined spectrophotometrically as per the quantitative filterpad method [21]. The partial yield factor for chlorophyll p_c is used from Section 2.1.3. Since we no longer expect the FQY to be wavelength-independent, the field application of the calibration is written as

$$\Phi_j = \frac{R_j}{k_j a_j^\star p_c}. \tag{8}$$

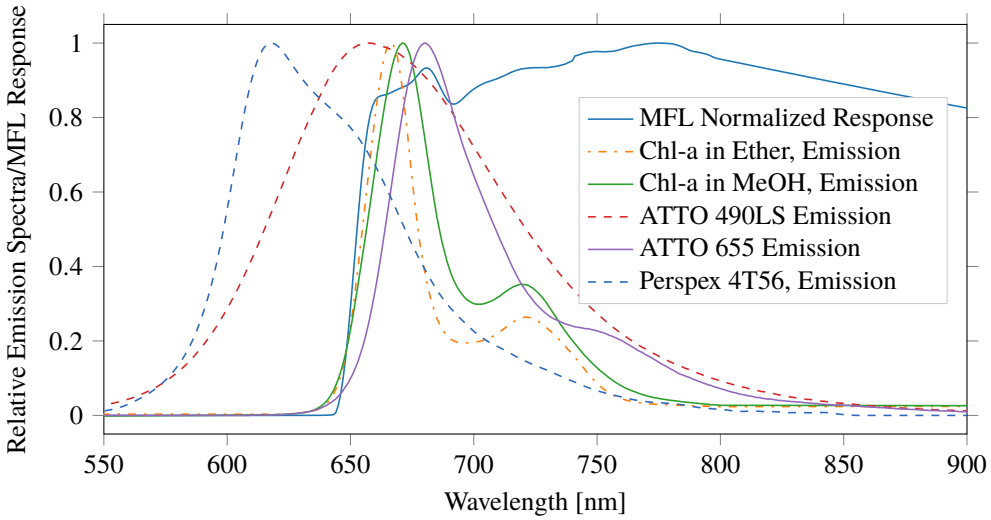

Fig. 2. Fluorophore normalized emission photon spectra plotted together with MFL normalized effective quantum detection efficiency.

2.3. MFL distance calibration

The distance calibration adds one dimension of complexity to the simple linear calibration model described above. Here we assume the observed fluid medium to be isotropic and homogeneous but now consider the primary stimulating radiation from the MFL arriving at and returned fluorescence signal from elementary plane-parallel layers of fluorescent medium as illustrated in Fig. 3.

The differential response dR of the MFL to a plane parallel layer of thickness dz at distance z was written as the product

$$\mathrm{d}R = a\Phi g(z)\mathrm{d}z, \tag{9}$$

Optics EXPRESS

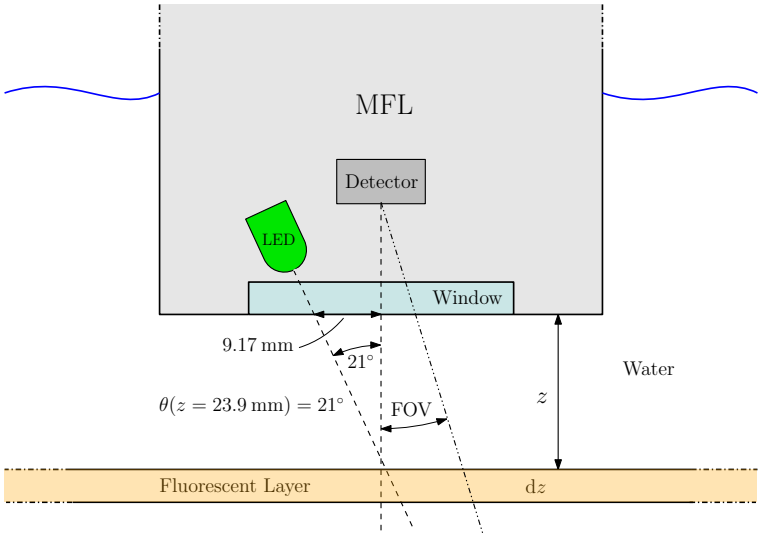

Fig. 3. MFL LED and detector viewing geometry. The angle at which the LED illumination intersects the fluorescent layer at distance z at the center of the MFL field of view (FOV) is θ.

where a is the absorption coefficient, Φ is the FQY and $g(z)$ is a function of distance z from the window of the MFL. The calibration function $g(z)$ subsumes all geometrical aspects of LED illumination and detector field of view, including the variation in illumination with distance. It was assumed to be unique and stable for each LED spectrum and independent of the characteristics of the fluorophore. Note that this is for an isolated layer of fluorescent material in an otherwise perfectly pure, transparent and infinite water body. The distance calibration setup was made as close to this ideal scenario as possible.

As in the case of the simple calibration model above, we introduced an indexing scheme to deal with different fluorophores with index i and different LED illumination spectra with index j. The differential MFL response was then written as

$$\mathrm{d}R_{ij} = a_{ij} p_i \Phi_i g_j(z) \mathrm{d}z, \tag{10}$$

which exhibits the assumption that the geometrical calibration function $g_j(z)$ is independent of fluorophore characteristics. The absorption coefficient a_{ij} is for fluorophore i and for LED j computed as a weighted integral as exemplified in Eq. (5). The MFL-relative partial quantum yield $p_i\Phi_i$ is used to take the actual MFL spectral response into account.

In practice, attenuation of the stimulating radiation in the layers preceding the layer under consideration must be considered, as well as the attenuation of the emitted fluorescence radiation which is returned to the detector. If scattering is neglected, on the outward path, the transmittance of the excitation radiation through the prior layers is

$$\mathcal{T}_{ij}(z) = \exp\left[-a_{ij} z \sec\theta(z)\right] \tag{11}$$

and on the return path, the transmittance of the emitted radiation is

$$\mathcal{T}'_i(z) = \exp\left[-a'_i z\right] \tag{12}$$

where a'_i is the effective absorption coefficient of the medium for the fluorophore emission

Optics EXPRESS

spectrum. Considering this outward and return absorption, the differential signal now becomes

$$\begin{aligned} \mathrm{d}R_{ij} &= a_{ij}p_i\Phi_i g_j(z)\mathcal{T}_{ij}(z)\mathcal{T}_i'(z)\mathrm{d}z \\ &= a_{ij}p_i\Phi_i g_j(z)\exp\left[-a_{ij}z\sec\theta(z)\right]\exp\left[-a_i'z\right]\mathrm{d}z \\ &= a_{ij}p_i\Phi_i g_j(z)\exp\left[-\left(a_{ij}\sec\theta(z)+a_i'\right)z\right]\mathrm{d}z. \end{aligned} \tag{13}$$

Integrating to obtain the total signal for a fluorescent medium layer of finite thickness t provides

$$R_{ij} = a_{ij}p_i\Phi_i\int_0^t g_j(z)\exp\left[-\left(a_{ij}\sec\theta(z)+a_i'\right)z\right]\mathrm{d}z. \tag{14}$$

The MFL distance response model described above is contingent on the assumption that the MFL has relatively narrow field of view (FOV). The FOV of the MFL was assessed by attaching a small piece of strongly fluorescent film to an opaque, black substrate and scanning this piece of film (immersed in pure dH_2O) across the MFL sightline at different distances. The full-width at half maximum (FWHM) of the linear FOV was thus established to be 16 mm at a distance of $z = 40$ mm and 24.3 mm at a distance of $z = 60$ mm. The half width at half maximum of the angular FOV which is illustrated in Fig. 3 was hence estimated to be 11.4°.

2.3.1. Acrylic fluorescent calibration plaque

A red-orange fluorescent plastic acrylic (Perspex 4T56) plaque, given index $i = 0$ and of physical thickness $t = 3$ mm, was used as a calibration artifact. The spectral absorption coefficient of the plaque was measured on the Cary 500 spectrophotometer. The emission spectrum and quantum yield Φ_0 of the plaque material were measured using a special experimental arrangement discussed in Section 2.3.5, after which the MFL-relative partial quantum yield factor p_0 was calculated. This plaque was found to saturate one or more LED channels of the MFL even at quite large distance. It was therefore necessary to attenuate the excitation radiation as well as the returned radiation using a neutral (gray) absorption filter, free of fluorescence, of thickness t_f and transmission $\mathcal{T}_{fj}$, respectively $\mathcal{T}_f'$ placed over the fluorescent acrylic plaque (Fig. 4). The outward signal is reduced by $\mathcal{T}_{fj}^{\sec\theta(z)}$ and the return signal by $\mathcal{T}_f'$, providing

$$R_{0j}(z_0) = a_{0j}p_0\Phi_0\mathcal{T}_f'\int_{z_0+t_f}^{z_0+t_f+t} g_j(z)\mathcal{T}_{fj}^{\sec\theta(z)}\exp\left[-\left(a_{0j}\sec\theta(z)+a_i'\right)(z-z_0-t_f)\right]\mathrm{d}z. \tag{15}$$

The gray filter spectral transmittance was measured using the Cary 500 spectrophotometer, allowing for calculation of $\mathcal{T}_{fj}$ and $\mathcal{T}_f'$ by weighted averaging. The calibration arrangement is shown in Fig. 4.The only unknowns in Eq. (15) are the functions $g_j(z)$.

2.3.2. Determination of $g_j(z)$

The calibration functions $g_j(z)$ were established to within a scaling constant d_i by using a thin film of fluorescent material (plastic in this case) bonded onto a flat, opaque, black, solid substrate. Performing the experiment in dH_2O, the response of the MFL was recorded as a function of the distance z between the fluorescent film and the front face of the MFL using a z-axis mechanical motion stage. The film was sufficiently thin that the total fluorescent signal could be regarded as arising at a single distance z of the film from the MFL. Two different films were used to verify independence of $g_j(z)$ from the fluorophore. The first film was given index $i = 1$, the second film was given $i = 2$ so that

$$R_{1j}(z) = d_{1j}g_j(z) \tag{16}$$

Optics EXPRESS

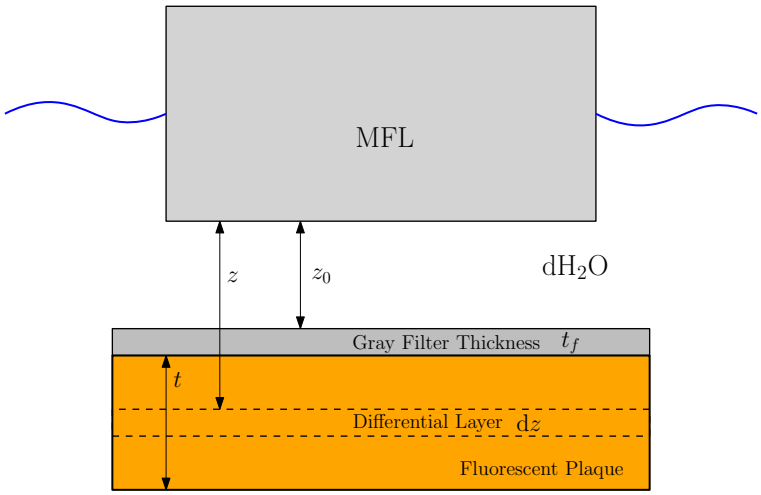

Fig. 4. Calibration setup using fluorescent acrylic plaque and neutral gray filter.

and

$$R_{2j}(z) = d_{2j} g_j(z), \tag{17}$$

where d_{1j} and d_{2j} are proportionality constants. Thus

$$g_j(z) = \frac{R_{1j}(z)}{d_{1j}} = \frac{R_{2j}(z)}{d_{2j}}. \tag{18}$$

The typical shape of the $g_j(z)$ functions was log-normal in character, starting at zero for $z = 0$, peaking roughly at $z \approx 15$ mm and then falling exponentially. For the 570 and 590 nm channels, the $g_j(z)$ functions exhibited an additional peak at closer range ($z \approx 6$ mm). The LED/detector geometry shown in Fig. 3 may suggest that the $g_j(z)$ should peak at $z \approx 24$ mm where the LED axes intersect the detector axis. However, the distance of peak response depends on this geometry as well as potential inverse-square decline in LED irradiance.

2.3.3. MFL calibration with fluorescent plaque

By measuring the response of the MFL to the gray filter with fluorescent plaque at different distances z_0, it is possible to obtain multiple simultaneous equations from Eq. (15), and rearranging to obtain the unknown scaling constant d_i. Substituting an option from Eq. (18) into Eq. (15) and solving for d provides

$$d_{1j} = \frac{a_{0j} p_0 \Phi_0 \mathcal{T}_f'}{R_{0j}(z_0)} \int_{z_0+t_f}^{z_0+t_f+t} R_{1j}(z) \mathcal{T}_{fj}^{\sec\theta(z)} \exp\left[-\left(a_{0j} \sec\theta(z) + a_i'\right)(z - z_0 - t_f)\right] \mathrm{d}z. \tag{19}$$

Everything on the right-hand side of Eq. (19) is known or measured, allowing calculation of d_{1j} and similarly d_{2j} or for further thin fluorescent films. It was found advisable to use larger z_0 as the calibration at close range became problematic, possibly due to detector nonlinearities and saturation effects as well as geometry errors. Since the detector is common to all LED channels, it is possible that if any LED produced measurements near or beyond saturation, this could impact the quality of other LED channel measurements. Any such MFL data were therefore discarded.

Optics EXPRESS

2.3.4. Calibration application

The distance calibration process was used to establish data for $g_j(z)$ through application of Eq. (19) and then returning to Eq. (18). Now, given a medium of unknown total FQY, but known MFL-relative partial yield factor, for example chlorophyll (p_c), and measured absorption coefficient a_j it becomes possible to apply the calibration to a set of field measurements R_j as follows. First a set of calibration factors G_j are computed using the field sample measured absorption data as

$$G_j = \int_0^\infty g_j(z) \exp[-(a_j \sec\theta(z) + a')z]\mathrm{d}z. \tag{20}$$

In practice, the upper limit of integration would be taken where the distance calibration functions $g_j(z)$ have dropped sufficiently low. In samples having low attenuation, the upper limit should be $z \gtrapprox 60$ mm. If measurements are performed in a bucket, the MFL should be placed considerably further than this from the bottom of the bucket and care taken that there is negligible fluorescence from the bucket material and minimal accumulation/settling of material in the bucket during measurements.

Finally, the unknown FQY was computed essentially by solving Eq. (14) and arriving at

$$\Phi_j = \frac{R_j}{G_j a_j^\star p_c}. \tag{21}$$

Since in field measurements we no longer assume that the FQY is independent of wavelength, the FQY now bears the LED index j. Note that in the low attenuation limit, the dye calibration factors k_j are related to the $g_j(z)$ as

$$k_j = \int_0^\infty g_j(z)\mathrm{d}z. \tag{22}$$

In order to obtain correct phytoplankton-specific FQY, it is necessary to know the phytoplankton-specific absorption. This involves estimation of absorption that is not attributable to phytoplankton e.g. detritus, dissolved organic matter. Note that radiative attenuation affecting the G_j factors is still calculated using the total absorption a_j of the sample. However, the $a_j^\star$ used in the final calculation in Eq. (21) must be the phytoplankton-specific absorption.

2.3.5. Plaque emission spectrum and quantum yield

The spectral absorption coefficient of the fluorescent calibration plaque was determined using the Cary 500 spectrophotometer. The emission spectrum and quantum yield Φ_0 were measured by irradiating the plaque with quasi-monochromatic light in the excitation wavelength region and then measuring the apparent spectral radiance of the plaque using a calibrated spectroradiometer. The first light source used was a high intensity blue LED (Osram OSTAR Projection LE B Q8WP) having typical peak emission at 455 nm. A second high intensity green LED (Osram OSLON LT CP7P) having typical peak emission at 521 nm was also used.

Analysis began with the spectral irradiance E_λ from the Osram LED on the plaque as illustrated in Fig. 5. This was measured with a calibrated B&W Tek SpectraRad spectral irradiance meter and verified with an ASD Inc. FieldSpec 3 spectroradiometer with a Spectralon white reference panel. All spectral radiant fluxes here are in photons per second per wavelength interval. There is a wavelength-dependent fresnel reflection providing a transmittance of $\mathcal{T}_F(\lambda) = 1 - \rho_F(\lambda)$ into the plaque. The plaque was assumed to have no internal scattering and the downward (as in Fig. 5) LED excitation photon irradiance within the bulk of the plaque would then decline

Optics EXPRESS

exponentially as

$$E_\lambda^{\downarrow}(z) = E_\lambda \mathcal{T}_F(\lambda) \exp\left[-a_o(\lambda) z\right], \tag{23}$$

where the z-coordinate is zero at the entrance surface of the plaque. Upon reaching the second face of the plaque, there is another fresnel reflection back into the plaque having upward irradiance

$$\begin{aligned} E_{F\lambda}^{\uparrow}(z) &= E_\lambda^{\downarrow}(t) \rho_F(\lambda) \exp\left[-a_0(\lambda)(t-z)\right] \\ &= E_\lambda^{\downarrow}(t)(1-\mathcal{T}_F(\lambda)) \exp\left[-a_0(\lambda)(t-z)\right], \end{aligned} \tag{24}$$

where t is the thickness of the plaque. The remaining excitation radiation exits from the plaque and is lost. If further internal fresnel reflections are neglected, the total LED excitation scalar irradiance within the plaque is

$$E_\lambda(z) = E_\lambda^{\downarrow}(z) + E_{F\lambda}^{\uparrow}(z). \tag{25}$$

Consider a cubical volume element within the plaque having sides of length Δz. The total spectral photon flux entering the volume element is $E_\lambda(z)\Delta z^2$, and the absorbed flux is $E_\lambda(z)\Delta z^2(1 - \exp\left[-a_0(\lambda)\Delta z\right])$. For small Δz, the absorbance can be approximated as $a_0(\lambda)\Delta z$ giving the incremental absorbed spectral photon flux (note the use of symbol Φ for optical flux) at coordinate z as

$$\Delta\Phi_\lambda(z) = E_\lambda(z) a_0(\lambda) \Delta z^3 \tag{26}$$

and the total number of absorbed photons per second over the specific band-limited spectrum expressed by E_λ between λ_1 and λ_2 is

$$\Delta\Phi(z) = \int_{\lambda_1}^{\lambda_2} E_\lambda(z) a_0(\lambda) \mathrm{d}\lambda \Delta z^3. \tag{27}$$

The limits of integration are dictated by the spectral limits of the stimulating Osram LED emission. The total emitted photon flux from the elemental volume is the product of the absorbed flux and the FQY calculated as

$$\Delta\Phi'(z) = \Phi_0 \int_{\lambda_1}^{\lambda_2} E_\lambda(z) a_0(\lambda) \mathrm{d}\lambda \Delta z^3 \tag{28}$$

where Φ_0 is the FQY of the acrylic plaque material. It was assumed that the emitted fluorescent flux is isotropic over 4π steradian, so the gain in emitted photon radiance per unit length in the limit as $\Delta z \to 0$ is

$$L_\star(z) = \frac{1}{4\pi} \Phi_0 \int_{\lambda_1}^{\lambda_2} E_\lambda(z) a_0(\lambda) \mathrm{d}\lambda. \tag{29}$$

The photon emission spectrum of the acrylic plaque material (Perspex 4T56) is shown in Fig. 2.

The photon path radiance within the plaque, for modest internal incidence angles φ from the z-axis is (since the incremental path length in direction φ is $\mathrm{d}z \sec\varphi$)

$$L_p = \sec\varphi \int_0^t L_\star(z) \mathrm{d}z. \tag{30}$$

The radiance that emerges from the plaque, L is scaled down by the square of the refractive index, n in the emission spectral region and subject to a last fresnel reflection loss, transmitting

Optics EXPRESS

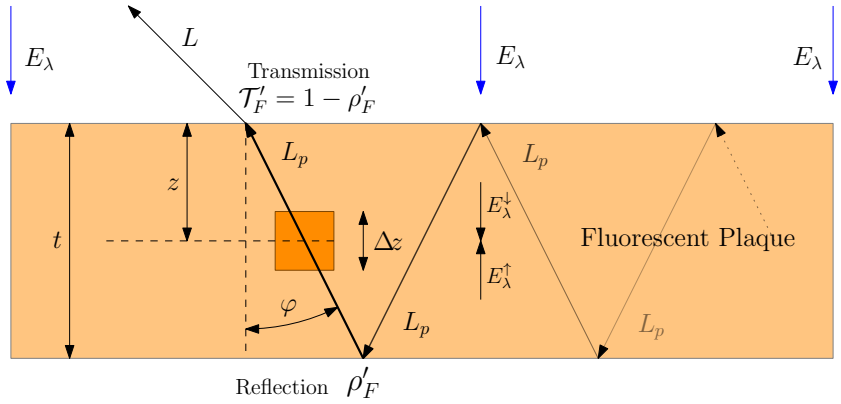

Fig. 5. The FQY measurement for the acrylic fluorescent plaque was performed by relating the emergent emitted radiance L to the FQY of the material and the incident excitation irradiance E_λ.

$\mathcal{T}'_F = 1 - \rho'_F$. However, there are additional internal reflections which contribute to the emergent radiance so that

$$\begin{aligned} L &= \frac{\mathcal{T}'_F}{n^2} L_p (1 + \rho'_F + (\rho'_F)^2 + (\rho'_F)^3 + \ldots) \\ &= \frac{\mathcal{T}'_F}{n^2} L_p \frac{1}{1 - \rho'_F} \\ &= \frac{1}{n^2} L_p . \end{aligned} \tag{31}$$

Substituting $L_\star(z)$ from Eq. (29) together with Eq. (30) and Eq. (31) provides

$$L = \frac{\Phi_0}{4\pi n^2} \sec\varphi \int_0^t \int_{\lambda_1}^{\lambda_2} E_\lambda(z) a_0(z) \mathrm{d}\lambda \mathrm{d}z. \tag{32}$$

The emergent photon radiance L was measured using the ASD Inc. FieldSpec 3 spectroradiometer. Hence, besides Φ_0, all variables in Eq. (32) are known or measured and the value of Φ_0 follows. Using this method, the FQY of the fluorescent acrylic plaque (Perspex 4T56) was determined to be 0.50 for the blue LED and 0.54 for the green LED. An average value of $\Phi_0 = 0.52$ was used. It is possible that there are multiple fluorophores in this acrylic material, which could make the FQY dependent on wavelength, but the blue/green discrepancy could also be due to measurement error.

3. Calibration results and discussion

3.1. Method comparison

The field-station FQY result presented in Section 4 computed from the three calibrations shows that the calibration using ATTO490LS typically produced the lowest estimates, with the distance/plaque calibration intermediate and the ATTO655 calibration producing the highest estimates, especially in the 570 and 590 nm channels.

Due to the large Stokes shift, the ATTO490LS calibration is thought to be more reliable. It is also more consistent with the distance/plaque calibration. While the acrylic plaque and the ATTO490LS dye solutions are essentially transparent in the MFL detection spectral region,

Optics EXPRESS

ATTO655 still has substantial absorption in the 640 to 700 nm region, which will inhibit response signal in the calibration scenario and cause artificially elevated FQY estimates in field application. This provides an argument that the calibration fluorophores should exhibit low absorption in the MFL detection spectral range, a condition not satisfied by ATTO655.

3.2. Calibration uncertainty

A full uncertainty assessment for both types of calibration is yet to be undertaken. Uncertainty in the quantum yield of the reference dyes and acrylic plaque feed directly into field sample FQY uncertainty. Besides other direct inputs to the calibration, a number of other factors could contribute to the uncertainty. The acrylic plaque has both large optical depth and strong variation of absorption coefficient with wavelength. This raises the possibility that there is significant failure of Beer's Law for quasi-monochromatic sources such as the LEDs in the MFL. This is most relevant when the acrylic plaque is placed particularly close to the MFL. This is a potential contributor to the discrepancies in results for the 570 and 590 nm channels of the MFL.

3.2.1. Scattering

Both forms of calibration described above are potentially compromised if used on samples having high optical attenuation, or with substantial scattering. The distance-dependent calibration method may be better suited to samples of higher attenuation or significant scattering. If the total spectral attenuation coefficient of the field sample is known, it could be used instead of absorption in Eq. (20). Adopting this approach would be equivalent to assuming that scattered photons are lost. Elevated values in the MFL backscatter channel at 880 nm could be used to flag samples with higher scattering.

4. Application example

The application of the two calibration methods to *in situ* oceanic data is presented in Fig. 6. The sample was collected from the Southern Ocean during the South African National Antarctic Expedition (SANAE 53) research cruise, onboard the *R.V. S.A. Agulhas II*, during the austral summer of 2013/2014. The MFL was continually exposed to surface water from the ship's underway seawater supply, as part of an onboard optics suite. Data were continuously recorded for 10 sec every 1 min, and averaged for 20 min over the time of the station. The corresponding total particulate absorbance was measured spectrophotometrically (Shimadzu UV-2501 PC, ISR-2200 internal integrating sphere), as per the quantitative filterpad method [21]. The non-algal particulate absorbance was measured [22], and absorption coefficients were determined [23]. The non-algal absorption was removed from the total particulate absorption to yield the phytoplankton-specific absorption $a_j^\star$.

The two different calibration methods show similarity, notably the ATTO490LS dye and the distance calibration, providing some evidence that the calibration procedure is robust. The relationship between calibration methods for 168 stations proved consistent (data not shown). The FQY describes the ratio of light fluoresced from PSII to that absorbed by both photosynthetic and non-photosynthetic pigments within the cell. The derivation of this apparent FQY for phytoplankton in their natural environment exploits the variable nature of phytoplankton-specific absorption and PS II fluorescence to potentially provide insight to the surrounding environment. Nutrient availability [14], light conditions [12] and taxonomy [11] all have a profound influence on the FQY of chl-*a*. Complementary nutrient, photophysiological, pigment and size data exists for all stations sampled on the SANAE53 cruise, however, interpretation of FQY variability is beyond the scope of this paper. These calibrations are designed to serve as a reproducible platform for the optical manipulation of similar instruments. The unique aspect of wavelength-specific FQYs provides insight into the dynamics of individual phytoplankton species, their photosynthetic efficiencies and thus their respective contributions to carbon export in our changing climate.

Optics EXPRESS

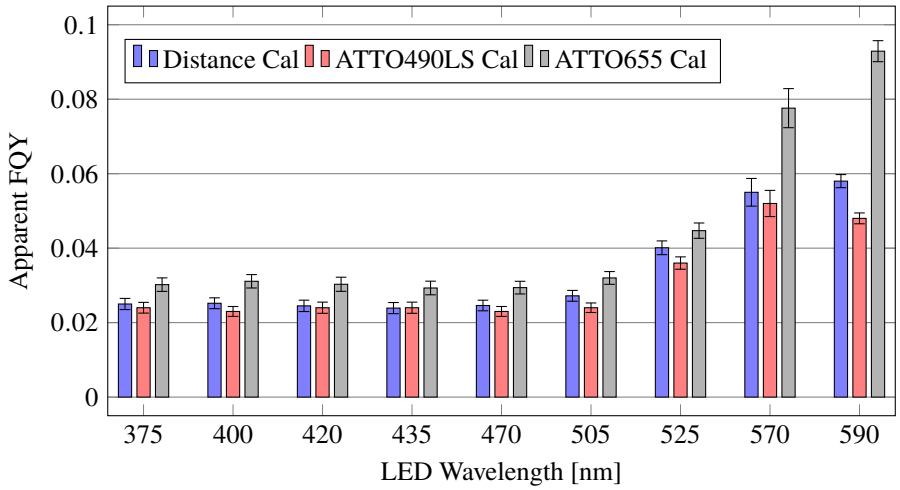

Fig. 6. Apparent FQY for *in situ* measurements. The error bars indicate the standard deviation of the field measurements, which would include all temporal variability of the sample as well as instrument noise.

5. Conclusion

A multi-excitation fluorometer has been calibrated for apparent fluorescence quantum yield using two methods and a number of fluorescent reference materials. The first method of calibration utilised fluorescent dye solutions of known FQY and the second made use of fluorescent plastic plaques and films. These methods are thought to be valid in the regime of low sample attenuation (absorption plus scattering), where the plaque method may be more applicable in higher attenuation situations. The derived FQY results from field measurements in the Southern Ocean are encouraging and largely consistent across calibration methods and materials. The inherent uncertainty of these methods and results is still to be quantified.

An instrument-type comparison would allow for development of a standardized calibration protocol for utilising multi-excitation fluorometers in FQY derivation. This improved instrument functionality will expand on the range of measurements captured by a single instrument. The thermostable MFL can be used to make individual acquisitions or record continuously over entire transects, allowing for routine measurements of FQY, concomitantly with species composition. The more field observations recorded, the more we can improve existing ocean colour FQY algorithms, allowing for continuous monitoring of phytoplankton dynamics in the global oceans.

Funding

Council for Scientific and Industrial Research (CSIR) Parliamentary grant (SNA2011112600001); Applied Centre for Climate and Earth Systems Science (ACCESS) National Research Foundation (NRF) grant (69461); South African National Antarctic Program (SANAP) NRF grant (SNA14073184298); University of Cape Town's Marine Research Institute (Ma-Re); Nansen-Tutu Centre for Marine Environmental Research, Ma-Re.

Acknowledgments

We thank JFE Advantech, Co. Ltd., for providing technical data on the MFL. In addition, we are grateful to Mr. Bertus Theron of CSIR for extensive help with many of the laboratory experiments, and to Drs. Thomas J. Ryan-Keogh and Marié E. Smith for their valuable input.

146.64.8.10 {ts '2019-03-22 10:22:47'}